Available online at www.sciencedirect.com
ScienceDirect
Acta Materialia 55 (2007) 6350–6355
Acta MATERIALIA
www.elsevier.com/locate/actamat

Synthesis and characterization of super hard, self-lubricating Ti–Si–C–N nanocomposite coatings

S.L. Ma [a,*], D.Y. Ma [a], Y. Guo [a], B. Xu [a], G.Z. Wu [a], K.W. Xu [a], Paul K. Chu [b]

[a] State Key Laboratory for Mechanical Behaviors of Materials, Xi'an Jiaotong University, Xi'an 710049, China
[b] Department of Physics and Materials Science, City University of Hong Kong, Tat Chee Avenue, Kowloon, Hong Kong, China

Received 5 June 2007; accepted 20 July 2007
Available online 14 September 2007

Abstract

Quaternary super hard Ti–Si–C–N coatings with different carbon contents were deposited on high-speed steel substrates by pulsed direct current plasma-enhanced chemical vapor deposition (PECVD) technology, using a gaseous mixture of $TiCl_4/SiCl_4/N_2/H_2/CH_4$/Ar. A variety of technologies have been employed to characterize the coatings, including X-ray diffraction, scanning and transmission electron microcopies, X-ray photoelectron spectroscopy, energy dispersive X-ray analysis, automated load–depth sensing and pin-on-disc. The super hard Ti–Si–C–N coatings were found to have unique nanocomposite structures composed of nanocrystallite and amorphous nc-Ti(C,N)/a-Si_3N_4/a-C and/or nc-Ti(C,N)/nc-$TiSi_2$/nc-Si/a-Si_3N_4/a-C, depending on the carbon contents in the coatings. The friction coefficient of the Ti–Si–C–N coatings with a higher carbon content (nc-Ti(C,N)/a-Si_3N_4/a-C nanocomposites) were found to be much lower than those of the Ti–Si–N coatings both at room and elevated temperatures, suggesting the formation of a graphite-like lubricious phase of amorphous carbon. However, they are still super hard (32–48 GPa) in spite of the carbon incorporation. This is due to a strong, thermodynamically driven and diffusion-rate-controlled (spinodal) phase segregation that leads to the formation of a stable nanostructure by self-organization. The energy difference between the grain boundary and the crystallite/amorphous phase interface hinders grain boundary mobility, leading to a gradual decrease in the grain size of the nanocrystallites. As a result, nanocomposite Ti–Si–C–N coatings with high hardness and a low friction coefficient can be produced. The coatings are foreseen to have high potential in dry and high-speed cutting tool applications, thus providing for cleaner, healthier and more pleasant machining conditions.

Keywords: Ti–Si–C–N coatings; Nanostructure; PECVD; Self-lubrication; Super hardness

1. Introduction

Conventional hard coatings, such as TiN and TiC, are commonly used to enhance the surface wear resistance of cutting tools [1,2]. However, their limited hardness, poor oxidation resistance and thermal instability at elevated temperatures in dry and high-speed cutting processes have spurred interests in ternary materials such as Ti–C–N, Ti–Al–N, Ti–Si–N and Ti–B–N [3,4], and also quaternary materials such as Ti–Al–Si–N [5]. Nanocomposite coatings consisting of nanocrystalline metal nitrides and amorphous phases, e.g. Si_3N_4 incorporated in Ti–Si–N(nc-TiN/a-Si_3N_4), in particular exhibit super hardness (40–105 GPa), high oxidation resistance (up to ~800 °C) and better thermal stability (up to ~1000 °C) in comparison with conventional hard coatings [6]. Unfortunately, the friction coefficient of these nanocomposite Ti–Si–N coatings is generally high (0.5–0.8) at both room and elevated temperatures [7], and so extra lubrication is needed in many applications. Problems involving the use of lubricants have become increasingly serious, especially when dry and high-speed cutting are demanded by the automotive, aerospace, domestic appliance and electronics industries. Indeed, there is increasing concern in all industrial sectors of the serious ecological and economical effects resulting from the use of

* Corresponding author. Tel.: +86 29 82668395; fax: +86 29 82663453.
E-mail address: slma@mail.xjtu.edu.cn (S.L. Ma).

1359-6454/$30.00
doi:10.1016/j.actamat.2007.07.046

cutting tool lubricants. This is because many lubricants present health hazards or are toxic, and some are even flammable. Hence, there is a need to develop new super hard coatings with better friction properties on a global basis.

Diamond-like carbon (DLC) is one of the super hard coatings with a low friction coefficient. However, the adhesion between the DLC coating and the substrate is usually poor. There is also inevitable adverse residual stresses in the coatings, especially for thicker ones deposited under energetic ion bombardment. Typically DLC also has crystalline lattice mismatch at the interface [8–10], therefore hampering wider applications in cutting tools. By adding various quantities of carbon to nanocomposite Ti–Si–N coatings, quaternary Ti–Si–C–N coatings with a nanocomposite structure may possess more desirable properties. However, research work on the design, synthesis, and characterization of these types of materials that possess both super hardness and low friction coefficients has been relatively sparse. Here, we report the synthesis of quaternary Ti–Si–C–N coatings with both super hardness and low friction coefficients (high wear resistance and self-lubrication). The effects of the carbon concentrations are evaluated and a mechanism is proposed to explain the relationship between the nanostructure and high hardness and low friction coefficients.

2. Experimental details

Ti–Si–C–N and Ti–Si–N coatings 5–6 μm thick were deposited on high-speed steel substrates by pulsed direct current plasma-enhanced chemical vapor deposition (PECVD) using a gaseous mixture of $TiCl_4$ (flow rate of 40 ml min^{-1}), $SiCl_4$ (5–15 ml min^{-1}), N_2 (400 ml min^{-1}), H_2 (800 ml min^{-1}), CH_4 (0–400 ml min^{-1}) and Ar (50 ml min^{-1}). $TiCl_4$ was bled into the vacuum chamber together with a H_2 carrier gas from the $TiCl_4$ tank at a temperature of 40 °C. $SiCl_4$ was introduced into the chamber from a $SiCl_4$ tank at room temperature. The PECVD system has been described elsewhere [11]. The substrate was placed on the charging plate (cathode of the system) and the substrate temperature, measured by a thermocouple, was kept at 500 °C during deposition. The wall of the chamber was the anode of the system and grounded. The pulsed voltage was 800 V and the frequency was 17 KHz.

X-ray diffraction (XRD) was conducted on the as-deposited surfaces using Cu Kα radiation to identify crystalline phases in the coatings, and the crystalline size was determined from the broadening by the Scherrer formula of the integral widths of the Ti(C,N) and TiN peaks. The coating thickness and structure were determined from cross sections using scanning electron microscopy (SEM). X-ray photoelectron spectroscopy (XPS) was used to determine the chemical states of silicon and carbon in the Ti–Si–C–N coatings. The elementary composition of the Ti–Si–C–N coatings was identified by energy dispersive X-ray analysis (EDS). The nanostructures of Ti–Si–C–N coatings were studied in details by plan-view transmission electron microscopy (TEM). The hardness measurements were performed using an automated load–depth sensing technique employing a Fischerscope 100 indentometer with a Vickers diamond indenter. A maximum load of 50 mN was used in order to assure that the indentation depth was within the 5–10% of the coating thickness. The hardness values obtained from the Fischerscope were verified by measuring the size of the remaining indentation utilizing SEM and calculating the hardness from the equation $H = 0.927\,L/A_P$, where L is the applied load and A_P is the projected area of indentation. Six repeated measurements were made for each specimen to obtain the average hardness.

The friction coefficients were evaluated using a pin-on-disc tribometer under a load of 5 N at a sliding speed of 20 cm s^{-1}. The tests were conducted using a 3 mm hardened (HRC 60–62) GCr15 steel ball as the counterpart at 25 and 550 °C and at 45% relative humidity in air without applying lubricants.

3. Results

Fig. 1 shows the X-ray diffraction patterns of the Ti–Si–C–N coatings with different carbon contents and low silicon concentration. The Ti–Si–C–N coatings exist as a Ti(C,N) solid solution when the carbon concentration is high (>29.3 at.%) and the preferred Ti(C,N) (200) crystal orientation appears. Other diffraction peaks from the crystalline phases such as $TiSi_2$ and Si are detected when the carbon content is lower than 29.3 at.%. A peak broadening phenomenon is observed with increasing carbon concentrations in the Ti–Si–C–N coatings. It is probably due to the smaller crystalline size and enhanced hardness produced via nanocrystalline hardening (to be discussed later). In

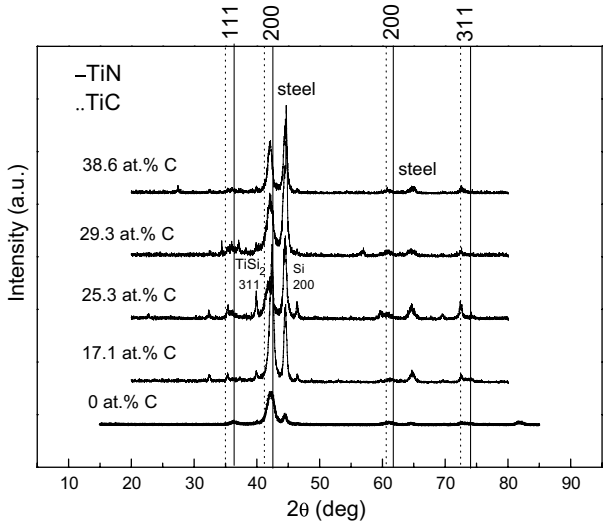

Fig. 1. X-ray diffraction patterns of Ti–Si–C–N coatings with silicon contents of 2.1–3.4 at % and different carbon concentrations.

comparison, the only crystalline phase found in the Ti–Si–N coatings is TiN in the absence of carbon (Fig. 1).

Some amorphous phases of a-Si_3N_4 and a-C in the Ti–Si–C–N coatings are revealed in the XPS spectra in Fig. 2. The Si2p spectrum in Fig. 2a. shows Si–N (102.6 eV), indicating the existence of Si_3N_4. However, the XRD results do not show any crystalline Si_3N_4 phase, implying that Si_3N_4 may be in the amorphous form (a-Si_3N_4). The C1*s* spectrum in Fig. 2b shows C–C (284.1–284.6 eV) and Ti–C (281.3–282.0 eV), demonstrating that some carbon atoms exist as amorphous carbon (a-C) because no carbon crystalline phase is indicated by XRD. Some carbon atoms replace nitrogen atoms in TiN crystalline lattice as Ti(C,N) and it may play a role in the increased hardness based on the rule-of-mixtures because the TiC is harder than TiN. In summary, two amorphous phases of a-Si_3N_4 and a-C exist in the Ti–Si–C–N coatings, whereas only one amorphous phase of a-Si_3N_4 is observed in the Ti–Si–N coatings [11].

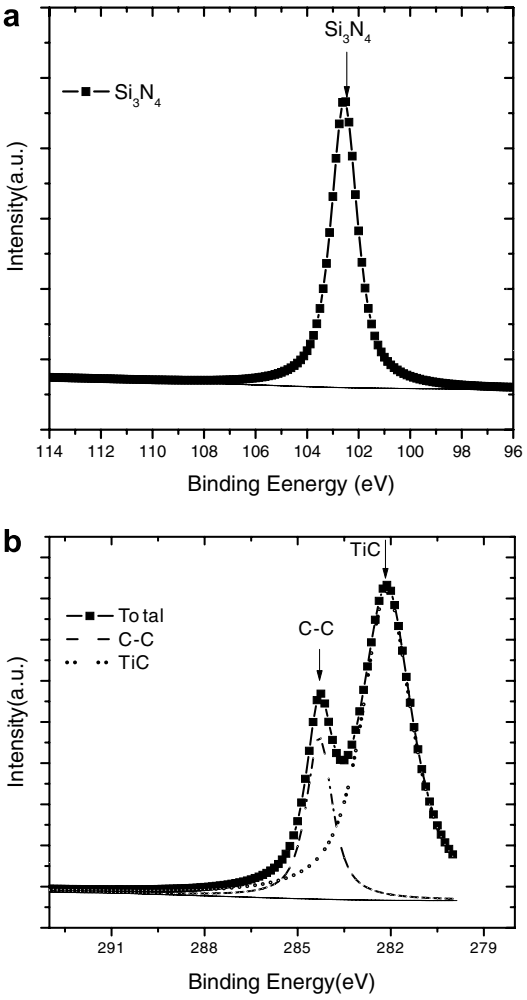

Fig. 2. Si2p and C1s XPS spectra acquired from the Ti–Si–C–N coatings with 25.3 at.% C and 2.3 at.% Si, indicating amorphous Si_3N_4 and carbon structures.

In order to investigate the structures in more details, TEM was conducted, and the plan view micrographs, together with the selected area electron diffraction (SAED) patterns of the Ti–Si–C–N coatings with low and high carbon contents and similar concentrations of silicon, are depicted in Fig. 3. The SAED patterns in Fig. 3a indicate the existence of crystalline phases of Ti(C,N), $TiSi_2$ and Si in the Ti–Si–C–N coating containing 17.1 at.% C, whereas Fig. 3b discloses only the crystalline phase of Ti(C,N) in the Ti–Si–C–N coating with 29.3 at.% C. The TEM results are consistent with the XRD results. The nanocomposite structure is shown in the high-resolution (HR) plan view TEM in Fig. 4, which also displays the SAED patterns. Nanocrystallites (black areas) with grain sizes of about 10–20 nm are embedded in the amorphous phases (white areas). The results suggest that the Ti–Si–C–N coatings with lower carbon concentration are composed of nc-Ti(C,N)/nc-$TiSi_2$/nc-Si/a-Si_3N_4/a-C, and the Ti–Si–C–N coatings with the higher carbon content are composed of nc-Ti(C,N)/a-Si_3N_4/a-C.

Fig. 5 shows the surface morphology and cross-sectional micrograph of the Ti–Si–C–N coatings. A typical non-columnar growth mode is indicated. The dense and fine microstructures which appear with the addition of carbon are believed to be responsible for the superior mechanical and chemical properties. As shown in Fig. 6, the crystalline size of the Ti–Si–C–N coatings containing 2.1–3.4 at.% Si decreases significantly from approximately 30 to 7 nm when the carbon concentration increases from 10 to

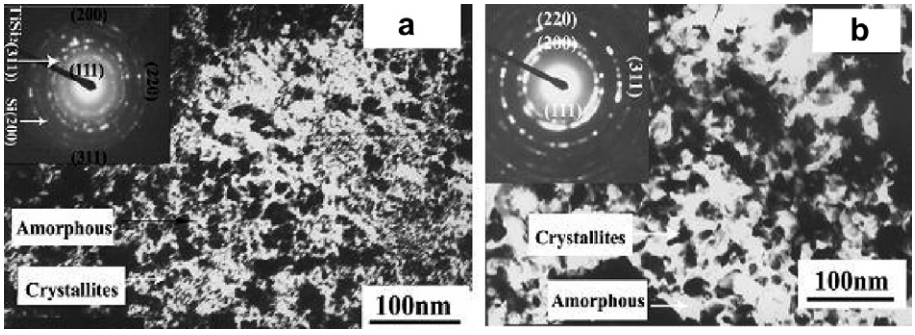

Fig. 3. Plan-view TEM nanocomposite images and SAED patterns obtained from Ti–Si–C–N coatings with: (a) 17.1 at.% C, 3.1 at.% Si and (b) 29.3 at.% C, 2.8 at.% Si.

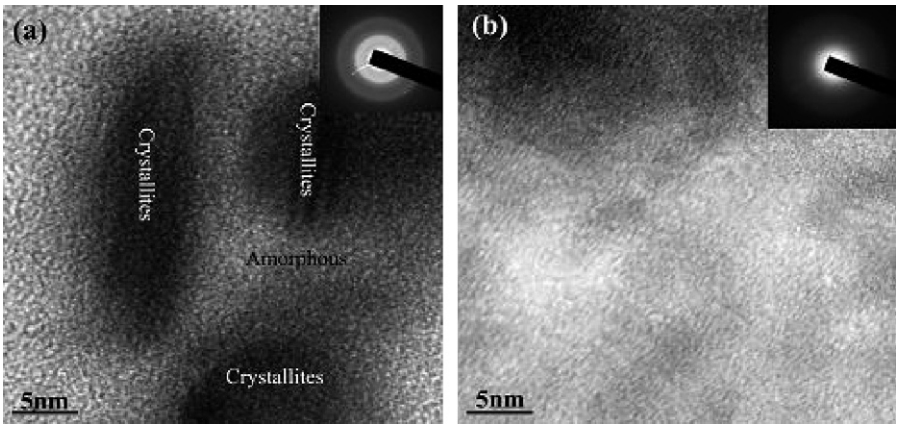

Fig. 4. Plan-view HR-TEM images and SAED patterns of Ti–Si–C–N coatings with 29.3 at.% C and 2.8 at.% Si: (a) nanocrystallites (black areas) and (b) amorphous phase (white areas).

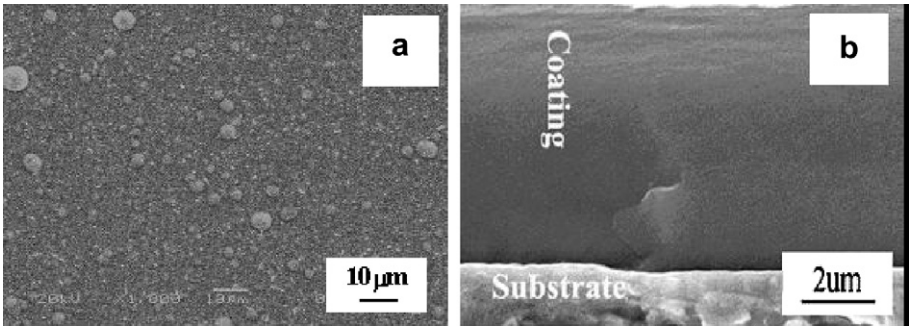

Fig. 5. Surface morphology and cross-sectional micrograph of the Ti–Si–C–N coatings with 29.3 at.% C and 2.8 at.% Si.

38.6 at.%, while the oxygen and chlorine impurity contents in the Ti–Si–C–N coatings determined by EDS are about 0.05 and 0.5 at.%, respectively. Consequently, the resulting Ti–Si–C–N coatings shows a super hard value of 32–48 GPa as measured by the nanoindentation techniques introduced earlier on. The hardness varies almost linearly with the carbon concentration due to a combination of nanocrystalline-size hardening and hardening increasing with carbon concentration according to the rule-of – mixtures in the f.c.c. Ti(C,N). In contrast, for the Ti–Si–N coatings, the hardness reaches a maximum and the crystalline size reaches a minimum at a silicon content of 13 at.%, as shown in Fig. 7. Afterwards, the hardness decreases gradually with increasing silicon concentration probably due to a diminished nanocrystalline-size hardening affect

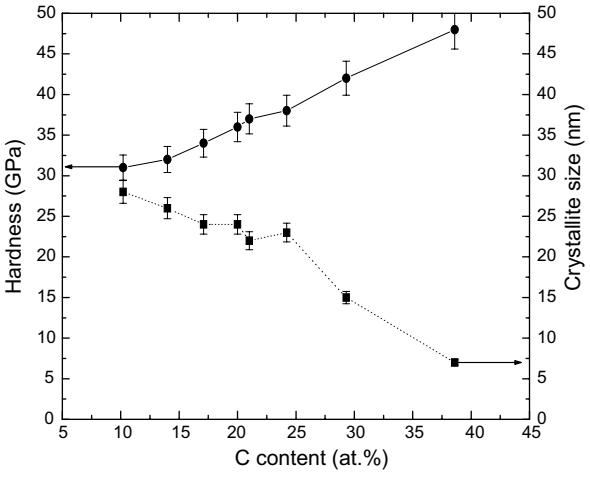

Fig. 6. Relationship between the crystalline size and hardness of the Ti–Si–C–N coatings with low silicon contents (2.1–3.4 at.%) with carbon concentrations.

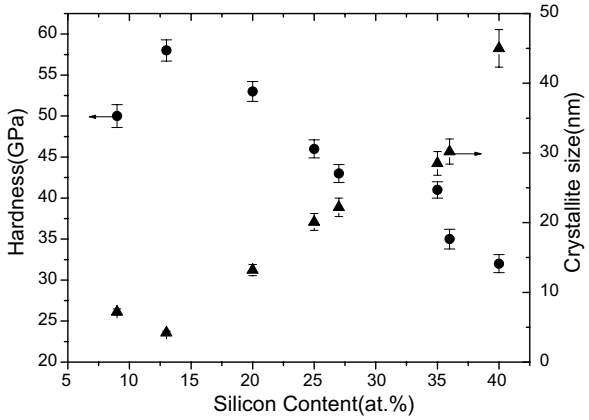

Fig. 7. Crystalline size and hardness of Ti–Si–N coatings with different silicon concentrations.

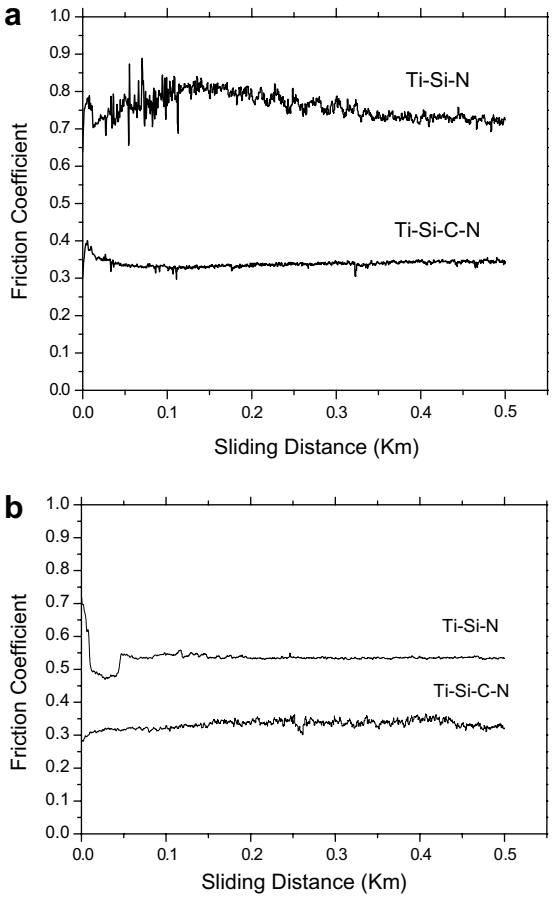

Fig. 8. Comparison of friction coefficients determined from the Ti–Si–C–N coatings (29.3 at.% C, 2.8 at.% Si) and Ti–Si–N coatings (3.0 at.% Si) measured at: (a) 25 °C and (b) 550 °C.

as larger nanocrystallites emerge. Therefore, as shown in Figs. 6 and 7, the dependence of the crystalline size and hardness on carbon concentration is different. The friction coefficients determined from the Ti–Si–C–N and Ti–Si–N coatings are shown in Fig. 8. Increased stability and lower friction coefficients are observed from the Ti–Si–C–N coatings at both ambient and elevated temperatures. For example, the friction coefficients decrease from approximately 0.75 for the Ti–Si–N coatings to 0.35 for the Ti–Si–C–N coatings at ambient temperature (Fig. 8a). The phenomenon appears to be related to self-lubrication arising from the formation of amorphous carbon acting as a graphite-like lubricating layer.

4. Discussion

The XRD and XPS as well as HR-TEM investigations have disclosed that incorporation of carbon into the Ti–Si–N coatings gives rise to unique nanocomposite structures composed of nanocrystallites embedded in an amorphous matrix. The formation is based on a strong, thermodynamically driven and diffusion-rate-controlled (spinodal) phase segregation that leads to the formation of the stable nanostructures by self-organization [12,13]. The spinodal nature of the phase segregation and the formation of the nanostructure are clearly supported by TEM in Figs. 3 and 4. The TEM micrograph in Fig. 3. shows a regular nanostructure that is typical of a spinodally segregated system. If the segregation and nanostructure formation have occurred by nucleation and growth, one would expect to see a much larger size distribution in the compositional modulation. Fig. 4 shows a high-resolution micrograph with a few nanocrystals, where the size of the nanocrystals, about 10–20 nm, agrees well with that determined from XRD results at carbon and silicon contents of 29.3 and 2.8%, respectively.

Liu et al. [14] have suggested that the energy difference between the grain boundary and crystallite/amorphous phase interface can give rise to the amorphous phase located at the boundary as seen in Figs. 3 and 4. Recently, Veprek et al. gave direct evidence which shows that a monolayer of Si_3N_4 interface is the most stable configuration, and its de-cohesion energy is higher than that of bulk Si_3N_4 [15]. It hinders the evolution of the grain boundary, and this effect is sensitive to the volume fraction of the amorphous phase that varies with the carbon concentration. This phenomenon is responsible for the grain growth restriction of the nanocrystallites, as shown in Fig. 6. This explanation is also valid for the relationship among the carbon content, grain size and hardness of the Ti–Si–C–N coatings when the silicon concentration is the same.

The nanocomposite coatings with self-lubrication are illustrated in Fig. 9, which presents a schematic of a nanocomposite coating design that exhibits self-lubrication and also super hardness, where an amorphous matrix carbon and a hard nanocrystalline phase were used to produce optimum mechanical performance and load support. Amorphous carbon was especially added to achieve structural adjustment of transfer films formed in friction contacts during dry/high sliding wear.

The mechanism suggested for this reduction in friction is the nanocomposite microstructure in which the small carbide grains present are thought to disrupt the atomic-bond

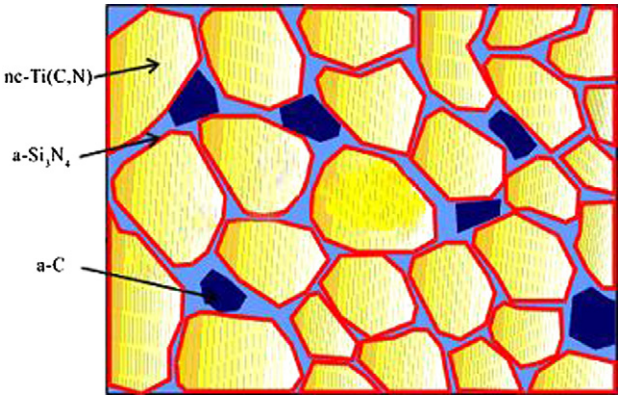

Fig. 9. Schematic of a nanocomposite coatings design for self-lubrication and super hardness.

continuity of the amorphous carbon, thus weakening its structural integrity and facilitating the release of carbon from the coating to the graphitization process. This conclusion is also supported by the carbon transfer from the coating to the counter surface as a solid lubricant [16]. Therefore, the improved friction and tribological properties accomplished with the Ti–Si–C–N coatings is related to the addition of carbon into the Ti–Si–N coatings, resulting in the formation of amorphous carbon, which acts as a graphite-like lubricating layer in the wear track surface structure. A graphite-like transfer film can be formed in the sliding contact and acts as a solid lubricating graphite structure; this self-lubrication mechanism leads to a large decrease in the friction coefficient. The reason for this is that the frictional force F is essentially a product of the shear strength S of the lubricant layer multiplied by the real contact area A, resulting from elastic and plastic deformation [17]: $F = S \times A$. Owing to the super hardness and significantly higher elastic module, the nanocrystallite Ti(C,N) is expected to have a much smaller contact area than metals under the same normal load. According to the equation above, a smaller contact area translates into a smaller frictional force when a lubricant layer of amorphous carbon is present. On the other hand, the friction coefficients of the Ti–Si–C–N coatings diminish continuously from about 0.35 at 25 °C to 0.30 at 550 °C (Fig. 8b), and those of the Ti–Si–N coatings decrease from about 0.75 at 25 °C to about 0.55 at 550 °C. This is probably due to the extensive graphitization, which is due to the higher temperature rise and strain energy, thus promoting graphitization [18]. On the other hand, the further reduction in the friction coefficient can be correlated to the formation of an amorphous oxidation resistant SiO_x layer on the surface of the Ti–Si–C–N coatings during the friction test at 550 °C [19]. SiO_x can also act as a lubricant layer in the chosen temperature range, further reducing the friction coefficients. Of course, as the temperature increases beyond a critical value, the viscosity of the SiO_x layer will reduce the lubricating efficacy and, consequently, the friction coefficients will increase again. However, this has not been confirmed since the highest temperature that can be achieved is 550 °C in the friction tests in the present study.

5. Conclusion

Superhard Ti–Si–C–N coatings consisting of nanocrystallites and amorphous microstructures of nc-Ti(C,N)/a-Si_3N_4/a-C and/or nc-Ti(C,N)/nc-$TiSi_2$/nc-Si/a-Si_3N_4/a-C have been fabricated by plasma-enhanced chemical vapor deposition. The impact of the carbon concentration on the microstructure and tribological properties of the materials have been investigated. The friction coefficients measured on the super hard Ti–Si–C–N coatings with high carbon concentrations (nc-Ti(C,N)/a-Si_3N_4/a-C) are lower at both room and elevated temperatures. This is because of the formation of a graphite-like lubricious phase which is composed of amorphous a-C. The coatings remain super hard in spite of the high carbon contents due to the formation of nanocomposite structures created by the segregation of the amorphous phase to the grain boundaries via a thermodynamically driven spinodal mechanism. This hinders the evolution of the grain boundary and leads to a gradual decrease in the grain size of the nanocrystallites. As a result, quaternary Ti–Si–C–N coatings with super high hardness and low friction coefficients can be produced, and these are thought to have great potential in dry and high-speed cutting tools.

Acknowledgements

This work was supported by the National Natural Science Foundation of China (Nos. 50671079 and 50531060), National Key Basic Research Project of China (No. 2004CB619302), and City University of Hong Kong Direct Allocation Grant 9360110.

References

[1] Rech J, Diouadi MA, Picot J. Wear 2001;250:45.
[2] Heim D, Hochreiter R. Surf Coat Technol 1998;98:1553.
[3] Veprek S, Reiprich S, Li SZ. Appl Phys Lett 1995;66:2640.
[4] Karvankova P, Veprek-Heijman MGJ, Azinovic D, Veprek S. Surf Coat Technol 2006;200:2978.
[5] Li YS, Shimada S, Kiyono H, Hirose A. Acta Mater 2006;54:2041.
[6] Veprek S, Heijman MGJ, Karvankova P, Prochazka J. Thin Solid Film 2005;476:1.
[7] Ma SL, Prochazka J, Karvankova P, Ma QS, Niu XP, Wang X, Ma DY, Xu KW, Veprek S. Surf Coat Technol 2005;143–148:194.
[8] Lohr M, Spaltmann D, Binkowski S, Santner E, Woydt M. Wear 2006;260:469.
[9] Morellit DT, Robinson CJ, Hartnett TM, Robinson CJ. Appl Phys Lett 1991;59:2112.
[10] Badzian A, Badzian T. Appl Phys Lett 1993;62:3432.
[11] Ma SL, Xu KW, Jie WQ. J Vac Sci Technol B 2004;22:1694.
[12] Karvankova P, Veprek-Heijman MGJ, Zindulka O, Bergmaier A, Veprek S. Surf Coat Technol 2003;163–164:149.
[13] Zhang RF, Veprek S. Mater Sci Eng A 2006;424:128.
[14] Liu ZJ, Shen YG. Acta Mater 2004;52:729.
[15] Veprek S, Veprek-Heijma MGJ. Surf Coat Technol 2007;201:6064.
[16] Daniel N, Fredrik S, Urban W, Sture H. Wear 2003;254:1084.
[17] Jahanmir S, editor. Friction and wear of ceramics. New York: Marcel Dekker, Inc, 1994. p. 137.
[18] Liu Y, Erdemir A, Meletis EI. Surf Coat Technol 1996:48–82.
[19] Jahanmir S, editor. Friction and wear of ceramics. New York: Marcel Dekker, Inc, 1994. p. 71.